7-2010

Pod of ultrasonic detection of synthetic hard alpha inclusions in titanium aircraft engine forgings

R. Bruce Thompson
Iowa State University

William Q. Meeker
Iowa State University, wqmeeker@iastate.edu

Lisa H. Brasche
Iowa State University, lbrasche@iastate.edu

POD OF ULTRASONIC DETECTION OF SYNTHETIC HARD ALPHA INCLUSIONS IN TITANIUM AIRCRAFT ENGINE FORGINGS

R. B. Thompson, W. Q. Meeker, and L. J. H. Brasche

Citation: AIP Conf. Proc. **1335**, 1533 (2011); doi: 10.1063/1.3592112

View online: http://dx.doi.org/10.1063/1.3592112

View Table of Contents: http://proceedings.aip.org/dbt/dbt.jsp?KEY=APCPCS&Volume=1335&Issue=1

Published by the American Institute of Physics.

POD OF ULTRASONIC DETECTION OF SYNTHETIC HARD ALPHA INCLUSIONS IN TITANIUM AIRCRAFT ENGINE FORGINGS

R. B. Thompson[2], W. Q. Meeker[1], and L. J. H. Brasche[3]

[1]Center for Nondestructive Evaluation and Department of Statistics, Iowa State University, Ames, IA 50011
[2]Center for Nondestructive Evaluation and Departments of Materials Science and Aerospace Engineering, Iowa State University, Ames, IA 50011
[3]Center for Nondestructive Evaluation, Iowa State University, Ames, IA 50011

ABSTRACT. The probability of detection (POD) of inspection techniques is a key input to estimating the lives of structural components such as aircraft engines. This paper describes work conducted as a part of the development of POD curves for the ultrasonic detection of synthetic hard alpha (SHA) inclusions in titanium aircraft engine forgings. The sample upon which the POD curves are to be based contains four types of right circular SHAs that have been embedded in a representative titanium forging, as well as a number of flat bottomed holes (FBHs). The SHAs were of two sizes, #3 and #5, with each size including seeds with nominal nitrogen concentrations of both 3 and 17 wt. %. The FBHs included sizes of #1, #3, and #5. This discreteness of the data poses a number of challenges to standard processes for determining POD. For example, at each concentration of nitrogen, there are only two sizes, with 10 inspection opportunities each. Fully empirical, standard methodologies such as $\hat{a}$ versus a provide less than an ideal framework for such an analysis. For example, there is no way to describe the beam limiting effect whereby the signal no longer increases the flaw grows larger than the beam, one can only determine POD at the two concentration levels present in the block, and confidence bounds tend to be broad because of the limited data available for each case. In this paper, we will describe strategies involving the use of physics-based models to overcome these difficulties by allowing the data from all reflectors to be analyzed by a single statistical model. Included will be a discussion of the development of the physics-based model, its comparison to the experimental data (obtained at multiple sites with multiple operators) and its implications regarding the statistical analysis, whose details will be given in a separate article by Li et al. in this volume.

Keywords: POD, Extrapolation, Hard Alpha Inclusion, MAPOD
PACS: 43.60.UV, 43.60.Cg, 81.70.Cv, 02.50.Sk

INTRODUCTION

Background

Probability of Detection (POD) is the metric whereby the efficacy of Nondestructive Evaluation (NDE) measurement techniques is quantified. It plays a variety of roles in structural integrity programs, including providing an input to the assessment of

Review of Progress in Quantitative Nondestructive Evaluation, Volume 30
AIP Conf. Proc. 1335, 1533-1540 (2011); doi: 10.1063/1.3592112

Design Target Risk (DTR) during the determination of the acceptability of new engine designs and the appropriateness of proposed field actions [1, 2]. Advisory Circular (AC) 33.14-1, "Damage Tolerance for High Energy Rotors," describes an acceptable means for showing compliance with the requirements of Section 33.14 of the Federal Aviation Regulations. AC 33.14-1 contains requirements applicable to the design and life management of high energy rotating parts of aircraft gas turbine engines. AC 33.14-1 is being updated based on experiences of the last decade. Default POD curves, such as those provided in AC 33.14-1 are intended to provide characteristic inspection capability that has been measured under typical, well controlled conditions. Such curves facilitate selection of NDE inspection techniques and corresponding lifing decisions. When properly applied, NDE inspection methods should result in similar capability. Since AC.33-14.1 was released in January 2001, there have been many advances in inspection technology

- The introduction of more sensitive inspection techniques based on greater focusing (e.g. Multizone)
- Improved statistical techniques to deal with imperfect data
- Improvements in physics-based models that can provide a guide to generalizing conclusions based on limited data (MAPOD)

The original default POD curves for titanium billet inspection have since been updated [3,4]. This paper describes recent efforts to update of the default POD curves for ultrasonic inspection to detect synthetic hard-alpha inclusions in titanium alloy forgings.

Challenges and Approach

Significant data for the NDE response of naturally occurring flaws in engine disk forgings are not available. Instead, the updated curves are based on measurements taken on a part that contains synthetic hard alpha defects and flat bottom holes with a limited number of sizes and nitrogen concentration levels. Multiple conventional and Multizone production inspections were performed on this part. A physics-based model of the measurement is used to allow a statistical model to be fit to all data simultaneously and to provide a basis for the necessary extrapolation (e.g. to describe beam limiting effects that are not adequately reflected in the data from a limited range of flaw sizes. The methods used take the SNR criteria of Multizone inspection into account.

THE SYNTHETIC INCLUSION DISK

The Synthetic Inclusion Disk (SID) contains 58 reflectors, as summarized in Table 1. Appendix A of [5] gives more detail on the locations of the reflectors. As an overview, at each of the five radial locations shown in Fig. 1, there are eight SHAs placed at different circumferential locations. These include two each of the four different types on SHAs shown in the table, one placed in a high noise region and one placed in a low noise region. The FBHs are placed near to the radial locations of the SHAs in the three regions in which the ultrasonic beam would enter through a flat surface normal to the disk axis.

TABLE 1. Reflectors in the SID block.

	# 1	# 3	# 5
3 WT %N SHA	0	10	10
17 WT %N SHA	0	10	10
FBH	12	3	3

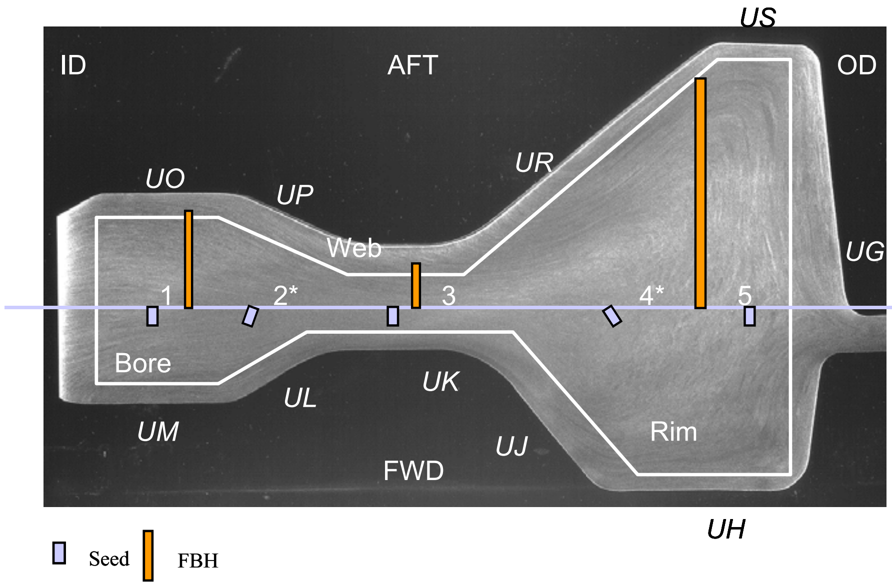

FIGURE 1. The SID with embedded seeds and FBHs.

THE INSPECTION TEST PLAN

For each inspection method, the SID was inspected at different sites and with different operators as summarized in Table 2, allowing an assessment of difference sources of variability. A more detailed description of decisions leading to this particular test plan is given in Section 3.5 of [5].

THE INSPECTION DATA

The SID disk was inspected with both conventional (two locations, six operators) and Multizone (three locations, seven operators) inspection methods. The responses from each measurement inspection were converted to Effective Flat Bottom Hole (EFBH). For this study, the EFBH response was defined as the flat bottom hole area that would give a signal response equal to the observed response, assuming calibration to a #1 flat bottom hole and was computed as EFBH = $(S/S_c)(\pi/4)(C/64)^2$ where S is the flaw signal strength (in units of % FSH), S_c is the calibration signal strength (in units of % FSH), and C is the size of the calibration hole (in units of 1/64 inch diameter). For the Multizone inspections, the noise threshold levels were also converted to EFBH units. Figure 2 provides a summary of the inspection data for both the conventional and the Multizone inspections. It is of interest to note the similarity between the Conventional and the Multizone inspection results.

TABLE 2. Number of operators per site for the two methods.

Inspection Method	Site A	Site B	Site C	Site D
Multizone	1 operator (all day shift)	2 operators (all day shift)	4 operators (all day shift)	
Conventional			3 operators (all day shift)	3 operators (on three different shifts)

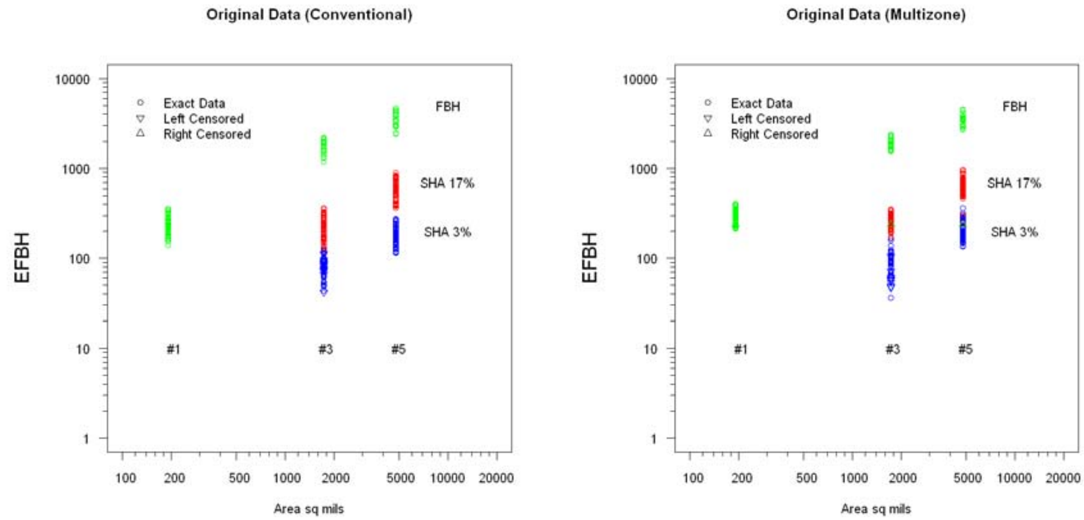

FIGURE 2. The amplitude values form the final data sets used in the analyses for Conventional (left) and Multizone (right) inspection.

Figure 3 compares the average measured value for teach target type and both inspection methods with a simple physics based model that ignores the beam-limiting effect and has no adjustable parameters. The model predictions are high for the #5 targets because of the beam-limiting effect. The model predictions are lower than expected for the 17% SHAs and this is believed to be due to diffusion of nitrogen into the titanium alloy matrix during the HIPping process when the SID was manufactured, leading to a small gradient of concentration near the ends of the SHA seed.

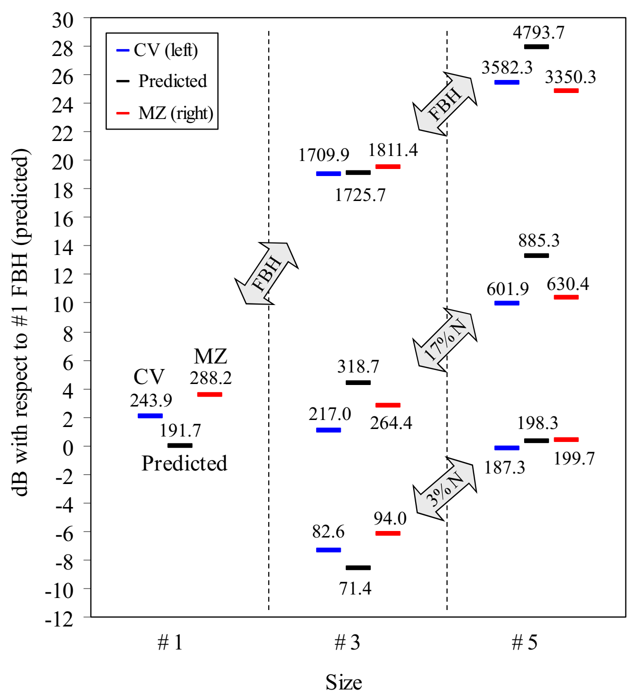

FIGURE 3. Comparison of predictions of theory (without beam limiting) to mean of the experimental data for all reflectors and both inspection procedures.

PHYSICAL MODEL

There are several limitations in the data that inhibit use of the traditional $\hat{a}$ versus a approach [6] of fitting a simple linear regression line relating log amplitude versus log target size to estimate POD. We know, e.g., that for planar reflectors like the SHAs and the FBHs in the SID, that once the reflector is larger than the beam, the signal would no longer increase. This is illustrated in Fig. 4. When the flaw dimensions become significantly smaller than the ultrasonic wavelength, the physics of the reflection changes, one enters the Rayleigh scattering regime, in which the pulse echo response of a planar reflector is proportional to flaw volume (area$^{1.5}$) rather than flaw area. This effect is illustrated in Fig. 4 and was discussed in some detail in previous work determining default POD curves for billets [4, 7].

The data points in Fig. 4 represent the responses measured from the 17 wt. %N SHAs in the SID in that previous study [8]. In that work, the inspection was performed under laboratory conditions at 10 MHz with a phased array specially designed with a large aperture to decrease the beam diameter in the focal plane to about half of the of production implementation of Multizone. Hence the data *are not* representative of the performance of the productions inspections whose performances are being quantified in this report. However, they *do* clearly illustrate the problem with applying the traditional $\hat{a}$ versus a approach under conditions in which the beam size is on the order of the size of the reflectors of interest. The dashed line is the result of the linear regression of that data, the first step in the $\hat{a}$ versus a approach. The solid line is an estimate of the behavior based on the inspection physics. An estimate of POD based on an inadequate straight-line model would be anti-conservative for both small and large size flaws. Thus an alternative approach is clearly needed.

A detailed description of physical theory that will provide an adequate model for estimation of POD in this setting is given in Appendix F of [5]. Here we provide an outline of the final model that was used. In this work, experimental measurements and the sizes of the SHA and FBH targets in the SID fall within the Kirchhoff regime. Thus in the following statistical modeling, only the Kirchhoff approximation is used where the signal (EFBH) is proportional to Reflectance of front surface, R. That is

$$\text{EFBH} = |R|\frac{\pi w^2}{2}\left(1 - e^{-2(b/w)^2}\right).$$

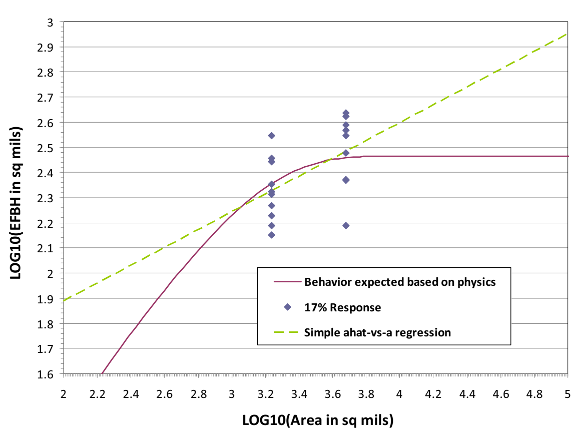

FIGURE 4. Comparison of $\hat{a}$ versus a based on regression analysis for data at two flaw sizes to results expected based on physics. These results are for measurements with an experimental laboratory system that is more tightly focused than current production inspections.

The beam limiting factor on the right-hand side of these expressions is a function of flaw radius b and beam radius w. By treating w as a tuning parameter reflecting the typical (unknown) beam radius, adding an overall fitting parameter α and taking log transformation we have:

$$\log_{10}\left[\mathrm{EFBH}(x)\right] = \log_{10}(\alpha) + \log_{10}\left[|R|\frac{\pi w^2}{2}\left(1-e^{-2(x/w)^2}\right)\right].$$

The reflectance factor R is controlled by change in acoustic impedance which is a predictable quantity as a function of %N. For flat bottom holes, R=1 and for the SHAs, based on experimental work described in [9],

$$R = R(\beta) = \frac{\rho_i v_i - \rho_m v_m}{\rho_i v_i + \rho_m v_m} \qquad (1)$$

where

$$\rho_m = 4461 \text{ kg/m}^3$$
$$v_m = 6175 \text{ m/sec}$$
$$\rho_i = \left(4490.9 + 5.03 \times N_{at} - 0.01 \times N_{at}^2\right) \text{ kg/m}^3$$
$$v_i = \left(6002.2 + 61.86 \times N_{at}\right) \text{ m/sec}$$
$$N_{at} = \frac{342 \times N_{wc}}{100 + 2.42 \times N_{wc}}.$$

where the last equation translated from (at%N) to (wt%N). To correct for the diffusion of some of the nitrogen into the titanium alloy matrix we used the following quadratic correction

$$N_{wc} = \left[1 - \beta \times \left(\frac{N_{\mathrm{w}}}{100}\right)^2\right] N_w$$

where N_w is the nominal weight percent nitrogen before the HIPping process and β is a tuning parameter that was estimated from the data.

RESULTS

This section presents estimates of mean response and POD for 3% (by weight) nitrogen SHAs, based on a statistical fitting of the physics-based model described in the previous section. Details of the statistical methods and predictions for other levels of percent nitrogen are available in Appendix G of [5]. The results of the analysis show that the Multizone inspection method has considerably better POD, in spite of the fact that the EFBH response estimates are similar. This difference is due primarily to the signal-to-noise ratio criterion employed in the Multizone method, in effect allowing a lower detection threshold in low noise regions of an inspected part.

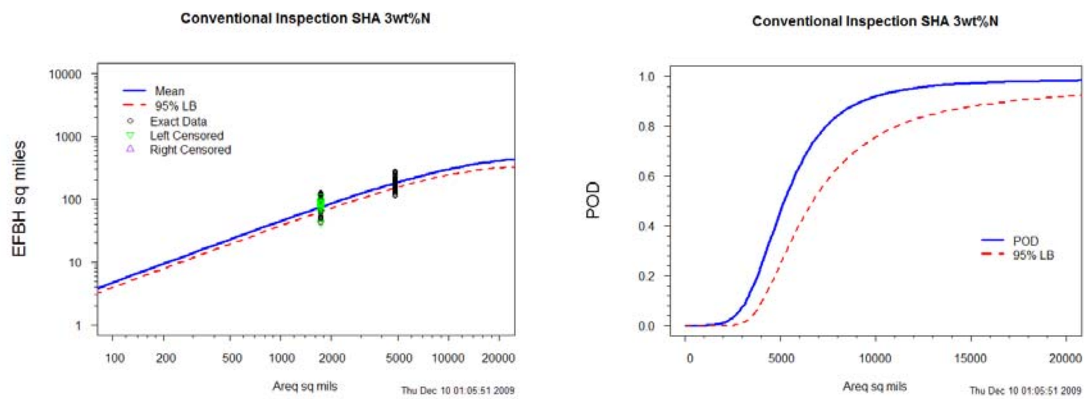

FIGURE 5. EFBH mean (left) and mean POD from Conventional inspection results as a function of target area for a 3% SHA.

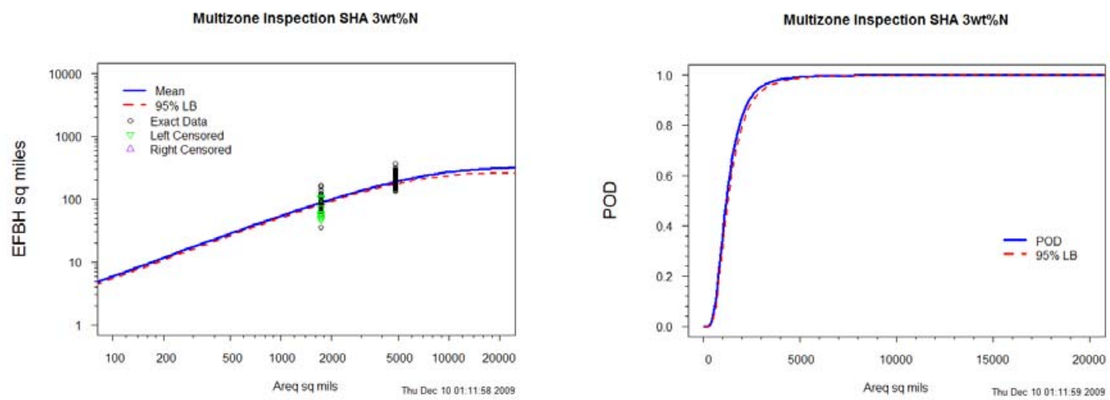

FIGURE 6. EFBH mean (left) and mean POD from Multizone inspection results as a function of target area for a 3% SHA.

FUTURE WORK

These POD curves are currently under review by the team and FAA. One key issue from the perspective of lifing is how to properly combine information from default POD curves based on naturally occurring defects (previous update of billet POD curves) and synthetic hard alpha inclusions (forgings) in a damage tolerant analysis. We expect that this future work will require some combination of physical modeling and experimentation.

ACKNOWLEDGEMENTS

This material is based upon work supported by the Federal Aviation Administration under Contract Number DTFACT-08-C-00005 and performed at Iowa State University's Center for NDE. We would also like to acknowledge the contributions of the participants in this project: General Electric: Rich Klaassen and Thadd Patton, Honeywell: Surendra Singh, Pratt and Whitney: Harpreet Wassan, Jeff Umbach, and Kevin Smith, Rolls Royce: Waled Hassan, Pramod Khandelwal, FAA: Cu Nguyen, Tim Mouzakis, Consultants to FAA: Jon Bartos, Floyd Spencer. The experimental results presented in this paper are

based on the efforts of the aforementioned team. However, as a final report has not been completed and approved by all, these results should be considered to represent the current views of the authors of this paper and not an endorsement by the total team or the funding agency.

REFERENCES

1. "Damage Tolerance for High Energy Turbine Engine Rotors," FAA Advisory Circular AC 33.14-1 (ANE 110, 1/8/01).
2. "Development of Anomaly Distributions for Aircraft Engine Titanium Disk Alloys"- Technical Paper presented by the AIA Rotor Integrity Sub-Committee at the American Institute of Aeronautics and Astronautics (AIAA) Conference in April, 1997.
3. R. Bruce Thompson and W. Q. Meeker, "Assessing the POD of Hard-Alpha Inclusions from Field Data," in Review of Progress in Quantitative Nondestructive Evaluation, Vol. 26B, D. O. Thompson and D. E. Chimenti, Eds. (AIP, NY, 2007), pp. 1759-1766.
4. R. Bruce Thompson, Bill Meeker, Mike Keller, Jeff Umbach, Thomas Chiou, Yurong Wang, Dick Burkel, Waled Hassan, Kevin Smith, Thadd Patton, and Lisa Brasche, "Update of Default Probability of Detection Curves for the Ultrasonic Detection of Hard-Alpha Inclusions in Titanium Alloy Billets," FAA Report DOT/FAA/AR-07/63, July 19, 2007.
5. R. B. Thompson, W. Q. Meeker, L. J. H. Brasche, R. Klaassen, J. Umbach, H. Wasan, W. Hassan, S. Singh, K. Smith, and T. Patton, "Update of Default Probability of Detection Curves for the Ultrasonic Detection of Synthetic Hard-Alpha Inclusions in Titanium Alloy Forgings." DOT/FAA/AR-xx/xx, Air Traffic Organization Operations Planning Office of Aviation Research and Development, Washington, DC 20591 (under review).
6. MIL-HDBK-1823A (2009), *Nondestructive Evaluation System Reliability Assessment*, Standardization Order Desk, 700 Roberts Avenue, Philadelphia, PA 19111.
7. R. B. Thompson, T. A. Gray, and W. Q. Meeker, "Use of Physics-Based Models to Guide the Extrapolation of Aircraft Engine POD Data to Small Flaw Sizes", in Review of Progress in Quantitative Nondestructive Evaluation, Vol. 25B, edited by D. O. Thompson and D. E. Chimenti, p. 1878, American Institute of Physics, Melville, NY, 2006.
8. F. J. Margetan, J. Umbach, R. Roberts, J. Friedl, A. Degtyar, M. Keller, W. Hassan, L. Brasche, A. Klassen, H. Wasan, and A. Kinney, "Inspection Development for Titanium Forgings", DOT/FAA/AR-05/46, Atlantic City, N. J.: Federal Aviation Administration William J. Hughes Technical Center, Airport and Aircraft Safety Research and Development Division May 2007.
9. M. F. X. Gigliotti, R. S. Gilmore, and L. C. Perocchi, "Microstructure and Sound Velocity of Ti-N-O Synthetic Inclusions in Ti-6Al-4V", *Metallurgical and Materials Transactions* A, 25, 2321-2329 (1994).